Icarus 197 (2008) 526–538

Contents lists available at ScienceDirect

Icarus

www.elsevier.com/locate/icarus

Fluvial erosion and post-erosional processes on Titan

Ralf Jaumann [a,b,*], Robert H. Brown [c], Katrin Stephan [a], Jason W. Barnes [c], Larry A. Soderblom [d], Christophe Sotin [e], Stephané Le Mouélic [e], Roger N. Clark [f], Jason Soderblom [c], Bonnie J. Buratti [g], Roland Wagner [a], Thomas B. McCord [h], Sebastien Rodriguez [e], Kevin H. Baines [g], Dale P. Cruikshank [i], Phil D. Nicholson [j], Caitlin A. Griffith [c], Mirjam Langhans [a], Ralph D. Lorenz [k]

[a] DLR, Institute of Planetary Research, Rutherfordstrasse 2, 12489 Berlin, Germany
[b] Department of Earth Sciences, Institute of Geosciences, Free University, Berlin, Germany
[c] Lunar and Planetary Laboratory, University of Arizona, Tucson, AZ 85721, USA
[d] US Geological Survey, Flagstaff, AZ 86011, USA
[e] University of Nantes, 44072 Nantes Cedex 3, France
[f] US Geological Survey, Denver Federal Center, Denver, CO 80225, USA
[g] Jet Propulsion Laboratory, California Institute of Technology, Pasadena, CA 91109, USA
[h] Bear Fight Center, 22 Fiddler's Rd., Winthrop, WA 98862-0667, USA
[i] NASA Ames Research Center, 245-6, Moffett Field, CA 94035-1000, USA
[j] Department of Astronomy, Cornell University, Ithaca, NY 14853, USA
[k] Space Department, John Hopkins University Applied Physics Laboratory, Laurel, MD 20723, USA

ARTICLE INFO

Article history:
Received 24 August 2007
Revised 30 May 2008
Available online 21 June 2008

Keywords:
Titan
Saturn, satellites
Satellites, surfaces
Spectroscopy
Geological processes
Ices

ABSTRACT

The surface of Titan has been revealed by Cassini observations in the infrared and radar wavelength ranges as well as locally by the Huygens lander instruments. Sand seas, recently discovered lakes, distinct landscapes and dendritic erosion patterns indicate dynamic surface processes. This study focus on erosional and depositional features that can be used to constrain the amount of liquids involved in the erosional process as well as on the compositional characteristics of depositional areas. Fluvial erosion channels on Titan as identified at the Huygens landing site and in RADAR and Visible and Infrared Mapping Spectrometer (VIMS) observations have been compared to analogous channel widths on Earth yielding average discharges of up to 1600 m^3/s for short recurrence intervals that are sufficient to move centimeter-sized sediment and significantly higher discharges for long intervals. With respect to the associated drainage areas, this roughly translates to 1–150 cm/day runoff production rates with 10 years recurrence intervals and by assuming precipitation this implies 0.6–60 mm/h rainfall rates. Thus the observed surface erosion fits with the methane convective storm models as well as with the rates needed to transport sediment. During Cassini's T20 fly-by, the VIMS observed an extremely eroded area at 30° W, 7° S with resolutions of up to 500 m/pixel that extends over thousands of square kilometers. The spectral characteristics of this area change systematically, reflecting continuous compositional and/or particle size variations indicative of transported sediment settling out while flow capacities cease. To account for the estimated runoff production and widespread alluvial deposits of fine-grained material, release of area-dependent large fluid volumes are required. Only frequent storms with heavy rainfall or cryovolcanic induced melting can explain these erosional features.

1. Introduction

The surface of Titan has been revealed globally, if incompletely, by the Cassini observations in the infrared and radar wavelength ranges as well as locally by the Huygens instruments. Extended dune fields, lakes, distinct landscapes, dendritic erosion patterns and deposited erosional remnants indicate dynamical surface processes (e.g. Tomasko et al., 2005; Lorenz et al., 2006, 2008a; Stofan et al., 2007). Valleys, small-scale gullies and rounded cobbles as observed at the Huygens landing site (Tomasko et al., 2005) require erosion and energetic motion to be formed. Hence, while a cryovolcanic origin of the observed erosion features cannot be excluded, the sharp bends and the branched networks of Titan valleys are more consistent with distributed sources than with localized sources which one would expected for cryovolcanic liquid release. Cryovolcanic flow features identified so far are also distinct from the observed branching channels (Lopes et al., 2007)

* Corresponding author at: DLR, Institute of Planetary Research, Rutherfordstrasse 2, 12489 Berlin, Germany. Fax: +49 3067055 402.
E-mail address: ralf.jaumann@dlr.de (R. Jaumann).

0019-1035/$ – see front matter
doi:10.1016/j.icarus.2008.06.002

and there is no apparent correlation of valleys and cryovolcanic features (Lorenz et al., 2008a).

Titan's surface temperature of 94 K constrain methane and ethane to be the only fluids that remain liquid for a considerable amount of time sufficient to alter the surface and only methane has a high enough vapor pressure to participate in a hydrological ("methanological") cycle (Lorenz et al., 2008a).

Models of Titan's atmosphere (Tokano, 2001; Hueso and Sanchez-Lavega, 2006) indicate that precipitating clouds of heavy atmospheric storms produce rain that reach the ground with rainfall of 110 kg/m^2 within 5–8 h (20–50 mm/h). On the other hand, average precipitation rates as estimated from the current atmospheric conditions might not exceed 1 cm/yr (Lorenz and Lunine, 1996; Lorenz, 2000; Rannou et al., 2006; Tokano et al., 2006), which is comparable to terrestrial deserts. To satisfy the energy balance of the hydrological cycle, the heavy rainstorms indicated above must be infrequent—perhaps centuries apart. On the other hand, if we assume a more gentle but steady drizzle (Tokano et al., 2006), long-term accumulation of liquid in the subsurface and lateral seepage processes might form extended reservoirs that might be released with high run-off rates, triggered by impact, tectonic or volcanic activity.

Size distribution from image-based grain counts at the Huygens landing site (Tomasko et al., 2005) indicate a median grain diameter of ~5 cm, with no grains larger than 15 cm and with a size range of 1–15 cm. Although it is not known whether this sediment is of fluvial origin, the rounding of larger grains and the moderate size sorting are consistent with fluvial transport (Perron et al., 2006). Gravel size grains are not reported from the landing site (Perron et al., 2006) and the smaller fraction of materials is of sand size because the Huygens probe landed on a relatively soft solid surface whose properties are analogous to wet clay, lightly packed snow and wet or dry sand (Zarnecki et al., 2005).

According to the scaling of sediment transport relations to the conditions on Titan by Burr et al. (2006), frictional shear velocities of 0.5–7 cm/s, unit discharge (mass flow rate per unit area or flow velocity times depth) of 0.005–8 m^2/s and shallow flow depth of 0.2–6 m at a slope of 0.001 seem to be sufficient to move grains of sizes between 0.1 mm–15 cm. Perron et al. (2006) constrain the precipitation rates needed to mobilize sediment of these sizes to 0.5–15 mm/h. In addition, high concentrations of sediment increase the concentration of the flow, decrease sediment-settling velocities and increase coarse grain transport up to the conditions of hyper-concentrated flows (Burr et al., 2006). The availability of large amounts of fine-grained organics on Titan (Elachi et al., 2005; Lorenz et al., 2006; Soderblom et al., 2007) suggests that hyperconcentrated flows might be possible on Titan. Thus, the observed channels, discharges, grain size distributions and runoff productions are consistent with expected surficial flow of sediment-loaded liquids on Titan.

In order to understand the fluvial processes in more detail we need to know whether these theoretical considerations for precipitation capacities and surface flow are reflected in the structure of Titan's erosional features such as valleys and channels and also if there is evidence for depositional processes. In the following the term 'channel' will be used for that part of a valley that actually confines flow of liquids.

2. Erosion by surface run-off

Valley-like features are known from the Huygens landing site and Cassini Imaging Subsystem (ISS; Porco et al., 2005), Visual and Infrared Mapping Spectrometer (VIMS) (Brown et al., 2004) and RADAR (Elachi et al., 2006) observations elsewhere (Porco et al., 2005; Tomasko et al., 2005; Stofan et al., 2006; Perron et al., 2006; Barnes et al., 2007a, 2007b; Lorenz et al., 2008a, 2008b; Table 1).

Table 1
Valley-like features as identified in VIMS and RADAR data (Barnes et al., 2007b; Porco et al., 2005; Stofan et al., 2006; Tomasko et al., 2005; Perron et al., 2006; Lorenz et al., 2008a; see also Fig. 1 for locations)

	Length	Width	Position	References
A	~100–200 km	800–2000 m	50° W/12° S	Barnes et al. (2007b)
B	<300 km	800–1000 m	123° W/9° S	Barnes et al. (2007b)
C	~50–100 km	800–2000 m	66° W/10° S	Barnes et al. (2007b); Lorenz et al. (2008a), T13, Fig. 7
D	~1000 km	10–20 km	Various, mainly south polar region	Porco et al. (2005)
E	10–200 km	500–1000 m	75° W/23° N	Stofan et al. (2006); Lorenz et al. (2008a), T3, Fig. 3
F	<5 km	17–100 m	192° W/10° S	Tomasko et al. (2005); Perron et al. (2006)
G	140 km	350–1400 m	140° W/8° S	This work
H	1200 km	1400–3000 m	192° W/10° S	This work
I	<50 km	<500 m	85° W/50° N	Lorenz et al. (2008a), TA, Fig. 2
J	<100 km	<3000 m	15° W/50° S	Lorenz et al. (2008a), T7, Fig. 5
K	<150 km	1–2 km	10° W/60° S	Lorenz et al. (2008a), T7, Fig. 6; speculative
L	>100 km	500–1000 m	345° W/75° N	Lorenz et al. (2008a), T25, Fig. 8

The location of theses features on Titan is indicated in Fig. 1. These valleys build dendritic and meandering systems a few hundred kilometers long and up to a few kilometers wide. However, due to the limited resolution outside the Huygens landing site, only the higher order and thus wider valley segments can be identified easily. Nevertheless, the lower order and thus smaller systems at the Huygens landing site justify the assumption that all scales of valley segments might exist also within the systems observed at lower resolution. Fig. 2 illustrates the characteristics of valley systems as observed by RADAR at low (192° W/10° S) as well as high (255° W/75° N) latitudes.

Surface conditions on Titan are different from those on Earth, yet the similarity between terrestrial and titanian fluvial features, especially at the Huygens site, suggesting comparable physical processes. An integrated model of precipitation, open-channel flow and sediment transport (Perron et al., 2006) supports the interpretation of the features at the Huygens landing site (Tomasko et al., 2005) as being formed by liquids and overland flow. Liquid methane (CH_4) is suggested to be the major fluid (Lunine, 1993). Its viscosity at 95 K is 1.8×10^{-4} Pa s, approximately five times lower than water at 298 K (9×10^{-4} Pa s) (Hanley et al., 1977; National Institute of Standards and Technology, 2005). Based on the work of Komar (1980) on martian fluvial sediment transport relative to sediment transport on Earth, Burr et al. (2006) considered similar relations for fluvial sediment transport on Titan and showed that flow velocities and minimum flow depth on Earth and Titan are within an order of magnitude of each other for a given grain size. Thus, liquid methane might be able to produce flows on Titan's surface that have at least comparable erosional power and sediment transport capacities as water on Earth. In addition, at the Huygens landing site the Huygens Decent Imager and Spectral Radiometer (DISR) observed water ice-rich sediment with rounded components (Tomasko et al., 2005) of a size that would reasonably be move as bed load on Titan (Burr et al., 2006). Given that fluvial processes are physically similar on Earth and Titan, a comparable morphology between terrestrial and Titan fluvial channels for similar amounts of input liquids should be expected, providing a first-order handle for calculating discharge from Titan fluvial channels using terrestrial empirical relationships (Burr, 2007). Volumetric or instantaneous discharge is an important parameter in fluvial geomorphology and of interest for quantifying the hydro-

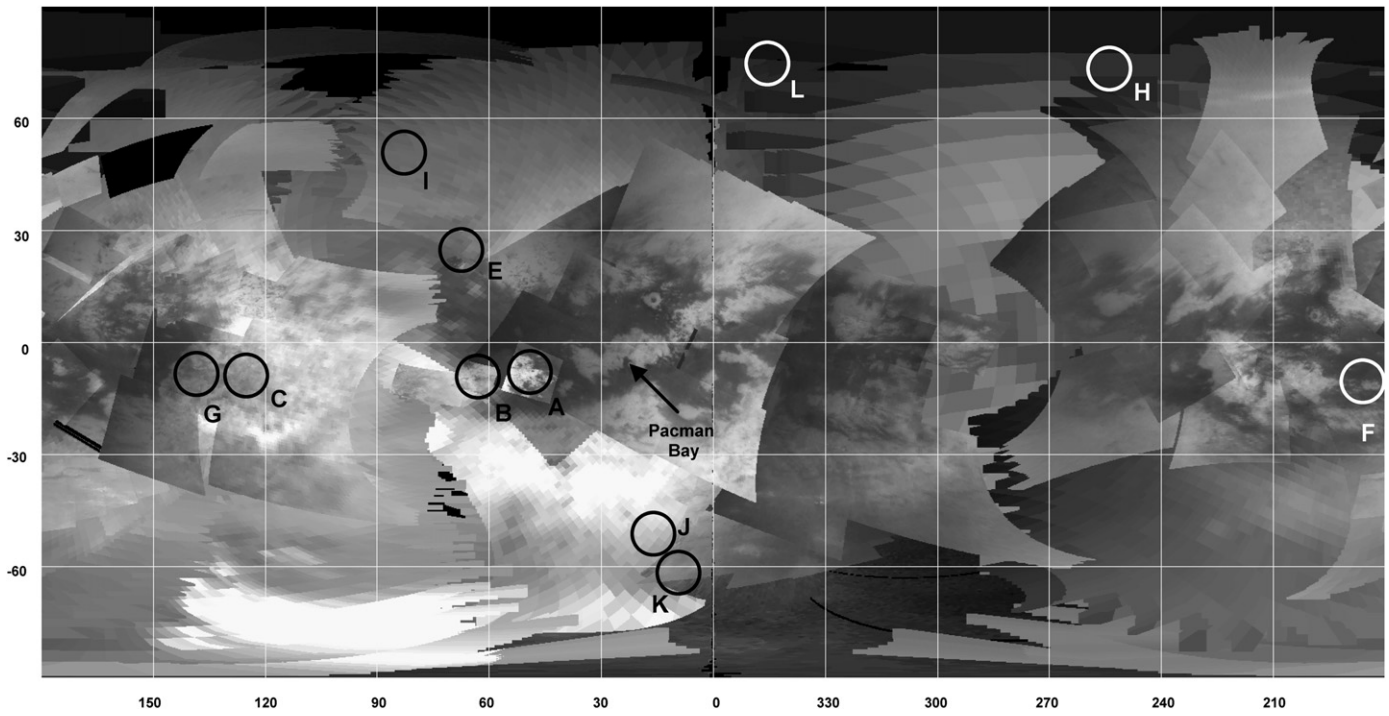

Fig. 1. Global map of Titan as derived from VIMS observations from orbits: 00A, 00B, 003, 005, 006, 017, 019, 020, 022, 023, 028, 029, 031, 036, 038, 040, 042, 045, 048, 049, 050. The circles indicate locations where valley systems have been identified in VIMS and RADAR data as well as at the Huygens landing site. The letters refer to Table 1 (see also Table 1 and Fig. 2).

logical cycle on Titan. It is a measure of the volume of liquid and sediment moved per time unit and can be estimated as the product of flow width, depth and velocity (Burr, 2007). The estimation of discharges allows constraining the amount of liquid that is needed to incise channel-like features of the observed shape and size. Based on production rates the surface runoff can be compared with atmospheric models in order to constrain precipitation rates.

Discharge of fluids is driven by gravity, and floods on Titan can be modeled to first order based on Earth-analogies for surface runoff, regardless of the composition of the fluid. On Earth, channel-sediment properties (that is, the size characteristics of material forming the channel perimeter) controlling the river width have a measurable effect on the geometry to discharge relations (Osterkamp and Hedman, 1982). Osterkamp and Hedman (1982) showed that channel width is related to discharge and an empirically derived multiple-power function best fits channel width W (m) to discharge Q (m^3/s) in a first-order approach for alluvial, unconfined channels carrying full-capacity flow for different recurrence intervals:

$$Q_r = aW^b. \tag{1}$$

Parameters a and b are dependent on the sediment properties and index r indicates the recurrence interval in years for periodic flood discharges. On Earth $a = 0.027$ and $b = 1.71$ for mean discharge, recurrence intervals of 1 year and averaged channel sediment characteristics including various proportions of silt, sand, gravel and cobble (Osterkamp and Hedman, 1982). Assuming comparable fluvial processes as on Earth, empirical data of terrestrial river width to discharge relations (Osterkamp and Hedman, 1982) may be scaled for extraterrestrial gravity (Irwin et al., 2005; Burr, 2007). On a lower gravity body, the same discharge requires a greater width and depth than on a higher gravity body in order to account for the lower flow velocity due to the smaller driving forces (Moore et al., 2003). To scale the empirical discharge equation to Titan's gravity, we used the approach proposed by Irwin et al. (2005) who combined the unit-balanced continuity equation and empirical Manning equation for channels that have a much greater width than depth:

$$Q = hWu = h^{5/3} S^{1/2} g^{1/2} W n^{-1}. \tag{2}$$

h, W, and u are the mean flow depth (m), width (m) and velocity (m/s), respectively. S is the slope, n the Manning roughness coefficient, and g the acceleration due to gravity with $g_T/g_E = 1.35\ m/s^2/9.807\ m/s^2 = 0.1376$. At the present time, there is little direct information on slopes on Titan but the relief ranges from less than one hundred meters to about 2000 m with slopes $<0.1°$ up to 37° at steep mountains (Elachi et al., 2005; Radebaugh et al., 2007; Barnes et al., 2007b). Thus, the assumption channel slopes on Titan are comparable with such on Earth is reasonable. In addition, other authors (e.g. Burr et al., 2006; Burr, 2007) rely on the same assumption.

Given the same discharge rate as for comparable slopes and with a channel-floor roughness similar to unconfined beds on Earth, W and h can be adjusted to the lower gravity on Titan by $Q_T = h'w'u'Q_E$, with $h'w'u'$ are conversion factors for depth, width, and velocity. In addition, depth h and width W are correlated empirically (William, 1988) by $h \approx W^{0.69}$. According to Eq. (2) $h' = 1.39$, $w' = 1.61$ and $u' = 0.46$. Thus, channels on Titan should have a depth, width and velocity of 1.39, 1.61 and 0.46 times, respectively, of those of unconfined, erosional channels on Earth. Therefore, a factor of 1.61^{-b} compensates for the greater width of channels on Titan in Eq. (1).

Kleinhans (2005) adjusted the discharge equation by substituting the relatively uncertain Manning coefficient n:

$$Q = hWu = \left(8gh^3W^3S\right)^{1/2}\left(f(W+2h)\right)^{-1/2}. \tag{3}$$

W, h, u, g, S are the same as for Eq. (2) except for the friction factor f (Silberman et al., 1963; Wilson et al., 2004; Kleinhans, 2005).

Following the same relative approach as for Eq. (2), we calculated the correction factors h', w', u' for depth, width and velocity

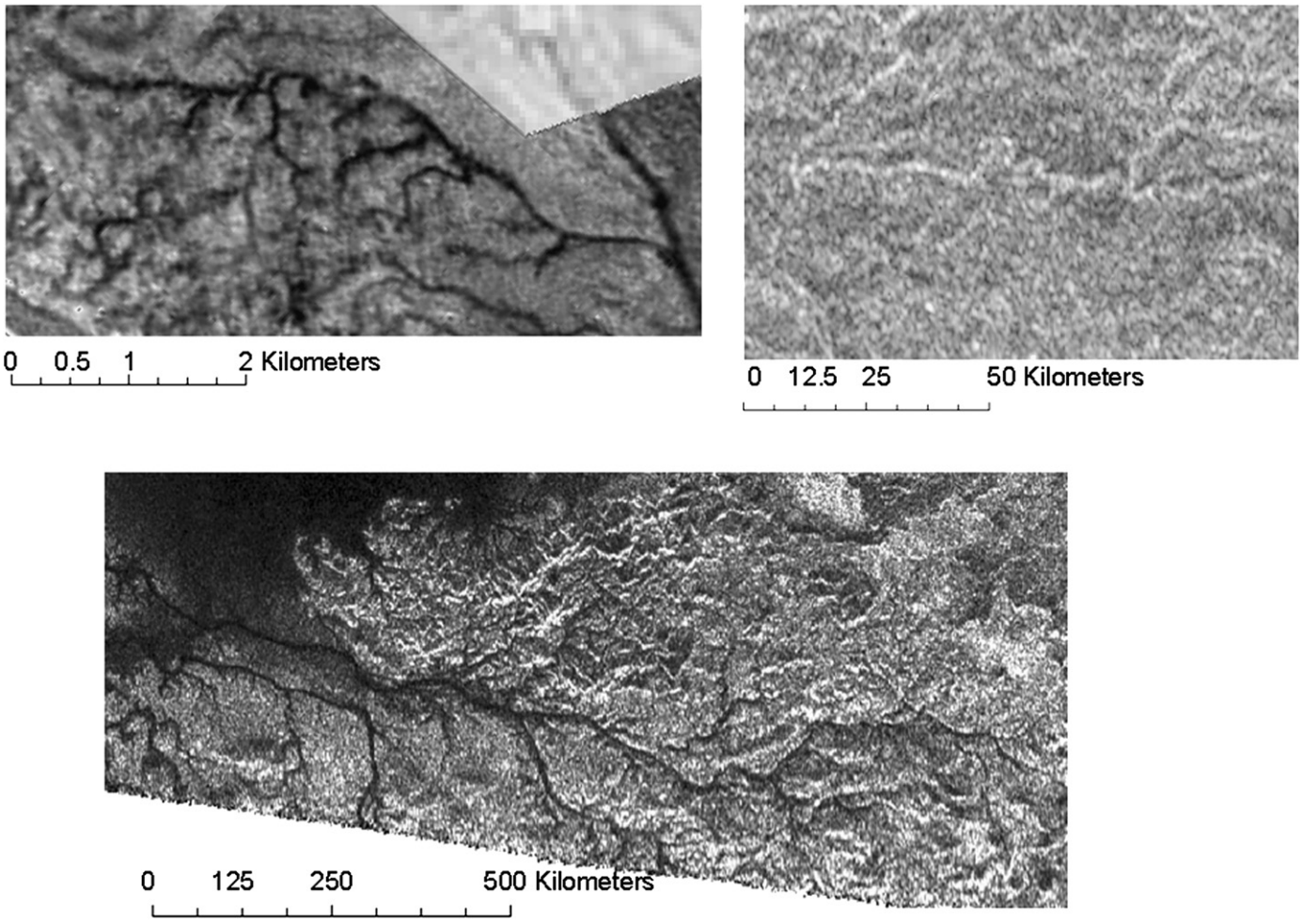

Fig. 2. Channels system at the Huygens landing site at 192° W, 10° S (DISR) (above right, F in Table 1), at 140° W, 8° (above left, G in Table 1) and 255° W, 75° S (below, H in Table 1) as identified in DISR images and RADAR observations of orbits T13 (350 m/pixel resolution) and T28 (1.4 km/pixel resolution). The channels systems are 5, 140 and 1200 km long and the channel widths within the systems range from the resolution limit of about 20 m at the Huygens landing site to 1400 m and 3000 m in the RADAR images, respectively.

with 1.40, 1.62 and 0.44, respectively. The resulting geometric parameters derived from the combination of unit-balanced continuity equation and empirical Manning equation as well as the independent discharge equation after Kleinhans (2005) coincide within less than 1%, indicating that the used scaling to Titan gravity is rather robust.

The presence of vast equatorial sand seas and dunes (Lorenz et al., 2006) requires enormous production and sedimentation rates of small particles that have mechanical properties comparable to terrestrial sands. In addition, the presence of cobbles at the Huygens landing site (Tomasko et al., 2005) also indicates fluvial transport of larger materials. Other sediment characteristics such as clay, silt or gravel-bedded channels, can also not be excluded.

We applied the width-to-discharge relation of Osterkamp and Hedman (1982) adjusted to Titan's surface conditions for sand-bedded and cobble-bedded sediment properties as well as for average sediment characteristic. On average, and for short recurrence intervals, discharges are higher by a factor of about 1.5–3 for cobble-bedded channels than for sand-bedded ones (Osterkamp and Hedman, 1982). At longer recurrence intervals this effect is reversed due to the tendency for increased attenuation of flood discharges in the downstream direction with increase of the recurrence interval (Osterkamp and Hedman, 1982). We did not account for gravel-only beds explicitly because gravel was not found at the Huygens landing site (Tomasko et al., 2005; Perron et al., 2006). However, without an accurate knowledge of the detailed channel sediment characteristics, it seems most feasible to rely on the average width-to-discharge relation as defined by Osterkamp and Hedman (1982) for mean discharge of averaged channel sediment characteristics including various proportions of silt, sand, gravel and cobble. Adjusted to Titan surface conditions these relation yield:

$$Q_{\text{av.}} = 0.0119 W^{1.71}. \quad (4)$$

Using the mean discharges for averaged channel sediment characteristics puts the estimates at a conservative lower limit.

The uncertainty in Eq. (4) is the estimation of the active channel widths. This is due to image resolution, the variability in channel widths and, in the case of more heavily incised channels, also the depth as well as a possible post-fluvial degradation that introduce potential errors amounting to a factor of about 3 (Irwin et al., 2005). In addition, possible errors of this order are inherent in empirical Eq. (1), because factors and exponents vary with the detailed channel sediment characteristics (Osterkamp and Hedman, 1982). These estimates are a conservative approach, making the model accurate within one order of magnitude that is comparable with the accuracy considerations by Burr et al. (2006).

So far we have no evidence that liquids are currently active on Titan, indicating that the channels might have been formed by liquid releasing events in the past. If we assume non-continuous but short periodic discharge events separated by recurrence intervals, discharge rates must increase to explain the observed erosion.

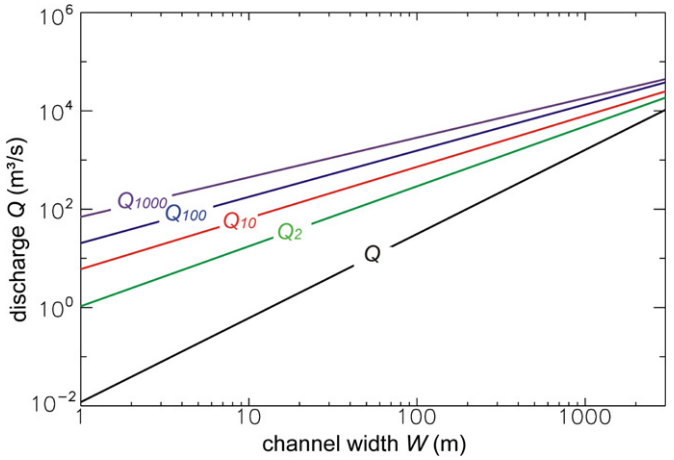

Fig. 3. Discharges adapted to Titan's surface gravity as derived from a discharge-to-channel width correlation from Osterkamp and Hedman (1982) for channels identified in VIMS and RADAR data and at the Huygens landing site (Table 1). The plot shows the discharge to width correlation for different recurrence intervals and for averaged channel sediment characteristics including various proportions of silt, sand, gravel and cobble.

Osterkamp and Hedman (1982) estimated for terrestrial rivers the following discharge to channel width correlation for recurrence intervals of 2, 10, and 100 years and an averaged channel sediment characteristics including various proportions of silt, sand, gravel and cobble:

$$Q_{av.2} = 1.9W^{1.22}; \qquad Q_{av.10} = 9.9W^{1.04}; \qquad Q_{av.100} = 32W^{0.94}, \tag{5}$$

with indices 2, 10, 100 indicating the recurrence interval and av. the average sediment characteristics, respectively. Following the same approach as discussed in Eqs. (2) and (3), the discharge to width correlation of Eq. (5) can be adjusted to Titan surface conditions yielding:

$$Q_{av.2} = 1.06W^{1.22}; \qquad Q_{av.10} = 6W^{1.04}; \qquad Q_{av.100} = 20.5W^{0.94} \tag{6}$$

and extrapolating these correlation to a recurrence interval of 1000 years yield

$$Q_{av.1000} = 69.8W^{0.81}. \tag{7}$$

The discharge to width correlation for different recurrence intervals on Titan is shown in Fig. 3.

In the usual case of non-bankfull flow, like on Earth, the dark branching valleys on Titan might be wider than the portion that has experienced fluid flow. The widths of dark valleys observed at the Huygens site vary between the resolution limit of the DISR instrument of 17 m/pixel and about 250 m (Tomasko et al., 2005; Perron et al., 2006). At the Huygens landing site DISR images indicate that the incised valleys are wider than the dark materials covering the channel floor by a factor of about 2 to 3 (Fig. 4). Assuming that only the dark parts of the valleys at the Huygens landing site are settled flood sediments then liquid might have covered no more than this width. This provides a rough estimate of the width ratio between valley features and actively flooded channel segments. According to this observation we assume that no more than 30–50% of the valleys have been active, which is comparable to active channel width on Earth (Osterkamp and Hedman, 1982). Choosing 30% for the active channel widths on Titan follows the conservative approach of this study. The estimated widths on Titan's valleys range from less than a few meters for the lower order channel segments as observed at the Huygens site (Perron et al., 2006) to about 3000 m for higher order segments (Table 1) and the active channels widths thus reach a few meters to about 1000 m.

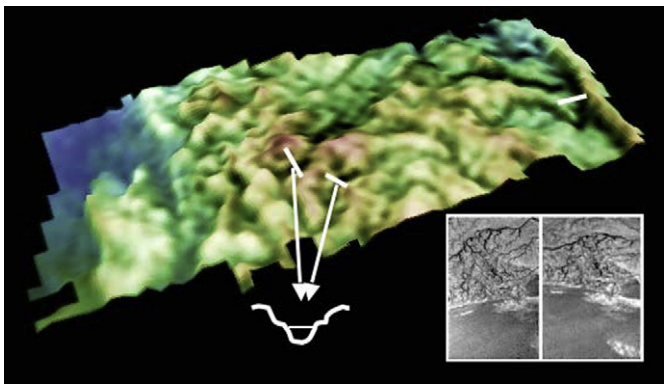

Fig. 4. Digital terrain model of the dendritic channel system at the Huygens landing site (adapted from Tomasko et al., 2005). Dark material only fills the deeper part of the channels indicating non-bankfull discharge. To first order approach only 1/3 to 1/2 of the channels might have been filled with liquid.

According to the estimated active channel widths, discharges for short recurrence intervals on Titan range from <1 m^3/s for the smallest identified channel segments (about 10 m wide) at the Huygens landing site to 1600 m^3/s for the highest order active channel segments (1000 m wide) of valley systems as observed in RADAR and VIMS data (Table 1). For longer recurrence intervals these values increase dependent on the channel width to 66 up to 7950 m^3/s for 10 years recurrence and to 178 m^3/s peaking at 13,510 m^3/s for 100 years recurrence, respectively (Table 2). For comparison with respect to short recurrence intervals (1 year), the Boulder river (Montana) at a width of 31.5 m has a mean discharge of 10.8 m^3/s, the Yellowstone river (Montana) at a width of 82.3 m has a mean discharge of 88.4 m^3/s, the Kansas river at a width of 223 m has a mean discharge of 138 m^3/s and the Missouri river at a width of 320 m has a mean discharge of 1370 m^3/s and at a width of 424 m 2260 m^3/s (Osterkamp and Hedman, 1982), while the Amazon river at a width of 22.9 km has a mean discharge of 212,500 m^3/s (Leopold et al., 1964).

Thus, discharges of active channels on Titan are consistent with the values needed to move sediment as estimated by Burr et al. (2006): unit discharges (mass flow rate per unit area or flow velocity times depth) of 0.005–8 m^2/s are needed to move 0.1 mm–15 cm particles; these values translate to 0.05–80 m^3/s discharge for 10 m channel width and 5–8000 m^3/s discharge for 1000 m channel width, respectively. Particularly the discharges for recurrence intervals >10 years as measured on Titan are consistent with these unit discharge values for sediment transport indicating at least periodic erosion events.

However in order to compare the erosional processes with the possible liquid release out of the atmosphere of about 110 kg/m^2 in 5–8 h or 20–50 mm/h (Hueso and Sanchez-Lavega, 2006) and the requested liquid release rates of 0.5–15 mm/h to move sediment of 1–15 cm size (Perron et al., 2006), estimates of the run-off production rates are needed.

The runoff production rate is defined by

$$P = Q/A, \tag{8}$$

where A is the drainage or catchment area, which is defined by the planform area covering the fine structure of the drainage network. The runoff production rate includes all liquid discharged in a channel regardless of whether it runs on the surface or is moved partly across the drainage area in the subsurface. Although the available resolution and the lack of detailed topographic information prevents the exact estimation of watersheds, connecting the starting

Table 2
Erosion parameters for selected channel systems on Titan

	Channel network at 140° W, 8° S (RADAR, T13)	Channel network at 255° W, 75° N (RADAR, T28)	Channel network at 192° W, 10° S (DIRS, Huygens landing site)
Length (km)	140	1200	5
Active width at mouth (m)	460	1000	10
Drainage area (km^2)	1500	58,000	3.7
Discharge at mouth (m^3/s)			
1 yr recurrence	420	1600	<1
10 yr recurrence	3540	7950	66
100 yr recurrence	6510	13,510	178
1000 yr recurrence	9770	18,270	446
Run-off production rate (cm/day)			
1 yr recurrence	2.5	0.2	1.5
10 yr recurrence	20.4	1.2	154.1
100 yr recurrence	37.5	2.0	415.6
1000 yr recurrence	56.3	2.7	1042.4
Run-off production rate (mm/h)			
1 yr recurrence	1.0	0.1	0.6
10 yr recurrence	8.5	0.5	64.2
100 yr recurrence	15.6	0.8	173.2
1000 yr recurrence	23.5	1.2	434.3

For comparison with respect to short recurrence intervals (1 year), the Boulder river (Montana) at a width of 31.5 m has a mean discharge of 10.8 m^3/s, the Yellowstone river (Montana) at a width of 82.3 m has a mean discharge of 88.4 m^3/s, the Kansas river at a width of 223 m has a mean discharge of 138 m^3/s and the Missouri river at a width of 320 m has a mean discharge of 1370 m^3/s and at a width of 424 m 2260 m^3/s (Osterkamp and Hedman, 1982), while the Amazon river at a width of 22.9 km has a mean discharge of 212,500 m^3/s (Leopold et al., 1964).

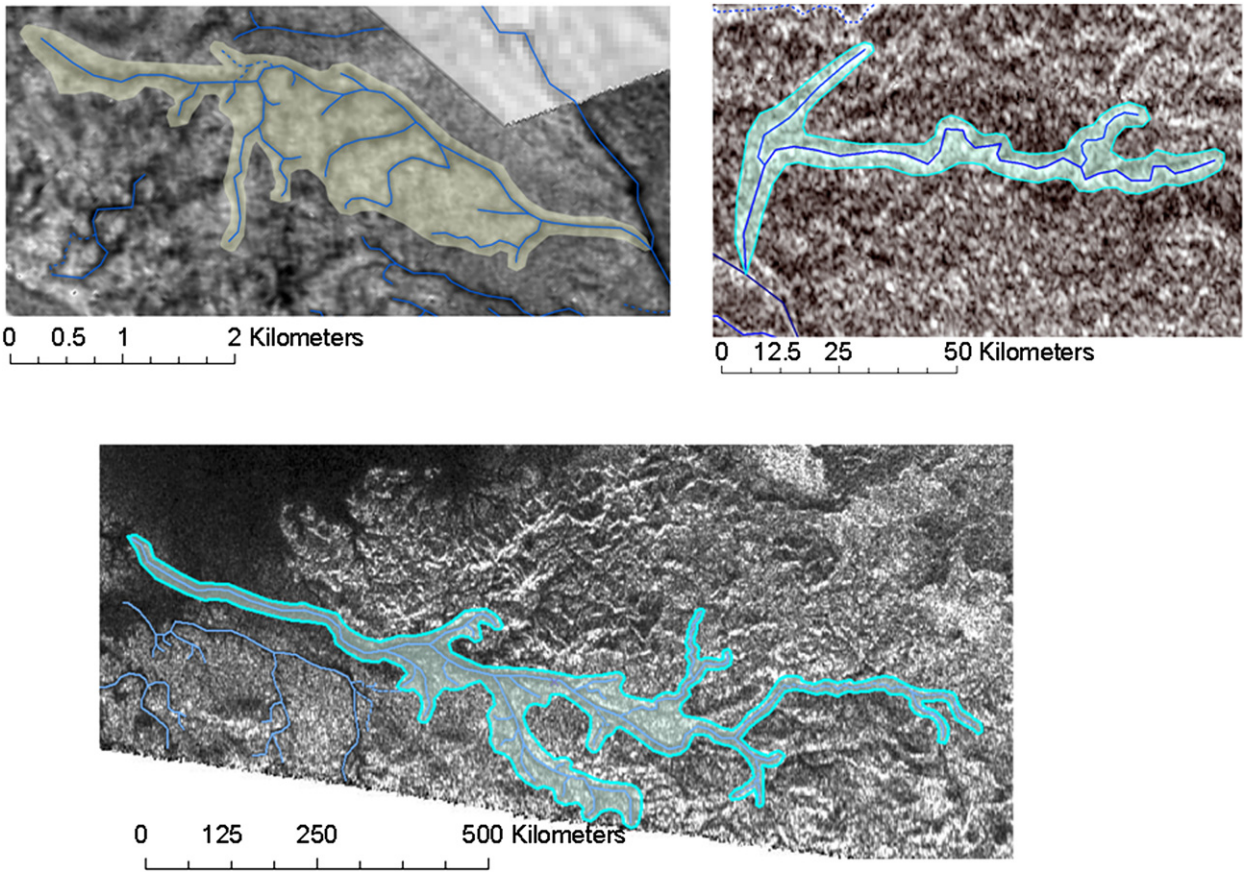

Fig. 5. Catchment areas of the channel networks at 140° W, 8° S (orbit T13), 255° W, 75° N (T28) and 192° W, 10° S Huygens landing site (see also Fig. 2 and Table 1).

points of the smallest recognizable tributaries define an area which to first order constrain the drainage area of a channel network (Fig. 5). However, information from radar backscattering or albedo properties indicating divides between tributaries is also used to constrain the size of drainage areas. In particular, the stereo model of the channels exposed at the Huygens site (Fig. 4) demonstrates that brighter ridges are dividing adjacent tributaries. Based on this approach, the drainage areas of the large dendritic channel systems as identified in RADAR observation at 140° W, 8° S (orbit T13) and at 255° W, 75° N (orbit T28) as well as of the smaller dendritic systems as observed in DISR observations at 192° W, 10° S (Huygens landing site) amount to 1500, 58,000, and 3.7 km^2, respec-

tively, covering different sizes of possible catchment areas. Run-off production rates are given in Table 2. Run-off production rates are highest in small low order channel network as at the Huygens landing site with small catchment areas and steep slopes. The observed cobbles at the Huygens landing site can be moved easily within a recurrence interval of about 10 years. For higher order systems such as at 140° W, 8° S (orbit T13) and at 255° W, 75° N (orbit T28) run-off production rates are significantly lower at short recurrence intervals (<1 mm/h) and reach about 50 mm/h within a 1000 years recurrence interval. However, in the wider, higher order channels, materials tend to be more crushed and segmented due to the longer transport history. Thus, even at the mouth of an extended valley system as observed by RADAR at 255° W, 75° N (orbit T28) sand and small cobbles of centimeter-size can be transported in reasonable times (<10 years). Nevertheless the results show that longer recurrence intervals are more realistic to explain the transport of large amounts of materials over large distances on Titan.

The existence of incised fluvial networks call for deposition zones where the eroded material came to rest somewhere on Titan. Alluvial plains such as the Huygens landing site (Tomasko et al., 2005; Soderblom et al., 2007) are likely candidates, although they are not widespread. Many radar-dark (and therefore flat and smooth) areas are seen close to the north polar lakes (Stofan et al., 2006) suggesting fine-grained sediments may be deposited in some abundance there. Lorenz et al. (2006, 2008b) argue that the bulk of the dune sands must be photochemical in ultimate origin, although this does not exclude some fluvial components. In addition, this view may change if further coverage finds more deeply incised valleys. In the following, we used VIMS data to search for the evidence of sedimentation zones by looking for spectral variations indicating changes in material and/or particle size distribution.

3. Post-erosional processes

Optical and spectral imaging of Titan's surface works throughout seven infrared spectral windows centered at 0.94, 1.08, 1.28, 1.58, 1.99, 2.77 and 4.93 µm with increasing transparency towards longer wavelengths. The Visible and Infrared Mapping Spectrometer (VIMS; Brown et al., 2004) achieves the best geological image performance in the 2 µm spectral region which appears the best compromise between signal-to-noise ratio (which declines with wavelength) and the transparency of the atmosphere (which increases with wavelength). VIMS ground resolutions in the infrared spectral region range between a few hundred meters and a few kilometers. This recalls the early days of Mariner 9 images, which for the first-time reveals small-scale scars on the martian surface that have been interpreted correctly as erosional even though the image resolution was not sufficient to prove their fluvial nature (McCauley et al., 1972).

The main optical characteristics of Titan's surface are bright and dark regions (Fig. 1). Comparisons with RADAR observations (Elachi et al., 2006) and measurements of the DISR (Tomasko et al., 2005) at the Huygens landing site indicate that at lower latitudes bright material is topographically high, whereas darker material tends to form lower-lying plains (Soderblom et al., 2007). Boundaries between the optically bright and dark areas are heavily frayed (Fig. 1). During Cassini's 20th Titan fly-by (October 25, 2006), VIMS observed a bright-dark boundary region at about 30° W and 7° S with a resolution of about 600 m/pixel (Fig. 6). A dark indentation informally called "Pacman Bay" by the VIMS investigators is covered by the highest resolution image with 500 m/pixel (Fig. 6). This, VIMS images of Titan's surface with the highest optical resolution to date provide the opportunity to investigate the nature of the bright-to-dark transition zone.

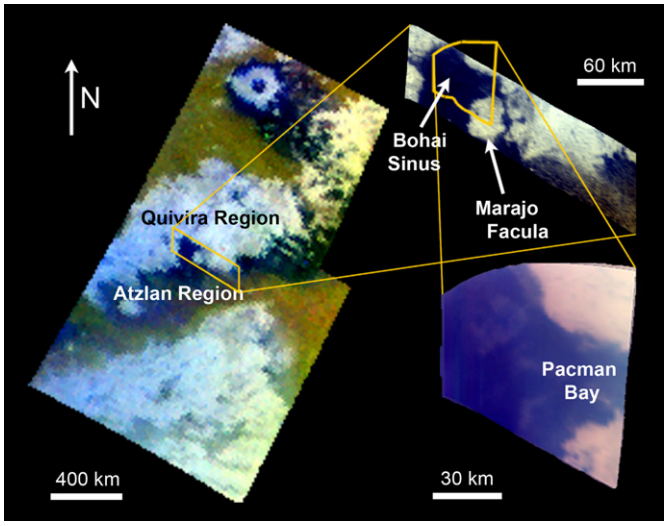

Fig. 6. On October 25, 2006 VIMS observed an area at 30° W and 7° S that marks the bright-dark boundary at a prominent indentation. Within the Bohai Sinus, a 25 km wide protrusion called "Pacman Bay" exhibits erosional and depositional details at a resolution of about 500 m/pixel. VIMS wavelength ratios at 1.29/1.08, 2.03/1.27 and 1.59/1.27 µm have been composed to generate blue, green and red color images in order to enhance the overall spectral contrast.

4. Observations

The VIMS data are calibrated radiometrically, i.e. the raw data number (DN) signal of each VIMS pixel is converted into physical values of reflectance (I/F). The specific energy (I_λ) is converted using the instrument's spectro-radiometric response function $R(\lambda)$ in photons per DN (Brown et al., 2004).

$$I_\lambda = \mathrm{DN}\tau^{-1}R(\lambda)hc\lambda^{-1}(A\Omega\delta\lambda)^{-1}, \tag{9}$$

where τ is the exposure time in seconds, h Planck's constant, c the speed of light, λ the wavelength of the particular VIMS bandpass, $\delta\lambda$ the size of the corresponding wavelength bin, A the area of the VIMS mirror, and Ω the solid angle subtended by a pixel in steradians.

The reflectance is finally obtained by dividing I_λ by a solar spectrum (Thekekara, 1973) with the solar flux at the instantaneous Sun–target distance, R_{-t}:

$$I/F = I_\lambda/F_{1,\lambda}(R_{-\oplus}/R_{-t})^2, \tag{10}$$

where $F_{1,\lambda}$ is the specific solar flux at 1 astronomical units $R_{-\oplus}$.

In addition, each VIMS pixel is geometrically rectified and converted into a map projected image cube in order to determine the geographic position of each pixel on Titan's surface. The spectral properties can be attributed to the geographic position and can thus be correlated with geological and geomorphological surface features. The projected cubes are combined into VIMS mosaics in order to produce spectral variation maps. In order to avoid changes to the original spectral signal, this re-projection is performed using the nearest-neighbor algorithm, which merely shifts a single VIMS pixel into the new location but does not interpolate between several VIMS pixels. The rectification and mosaicking process of VIMS cubes is described in detail in Jaumann et al. (2006).

Short exposure times (<80 ms) are needed to make observations at closest approach and this results in a lower signal-to-noise ratio. In order to increase the signal-to-noise we used a principal component transformation (PCT) or Karhunen–Loève transformation (KLT; Rothery and Hunt, 1990; Richards, 1994) and co-adding of channels. VIMS acquires images in 352 contiguous spectral channels. Thus, the number of spectral channels is much higher than the intrinsic variability of the observed components of a given

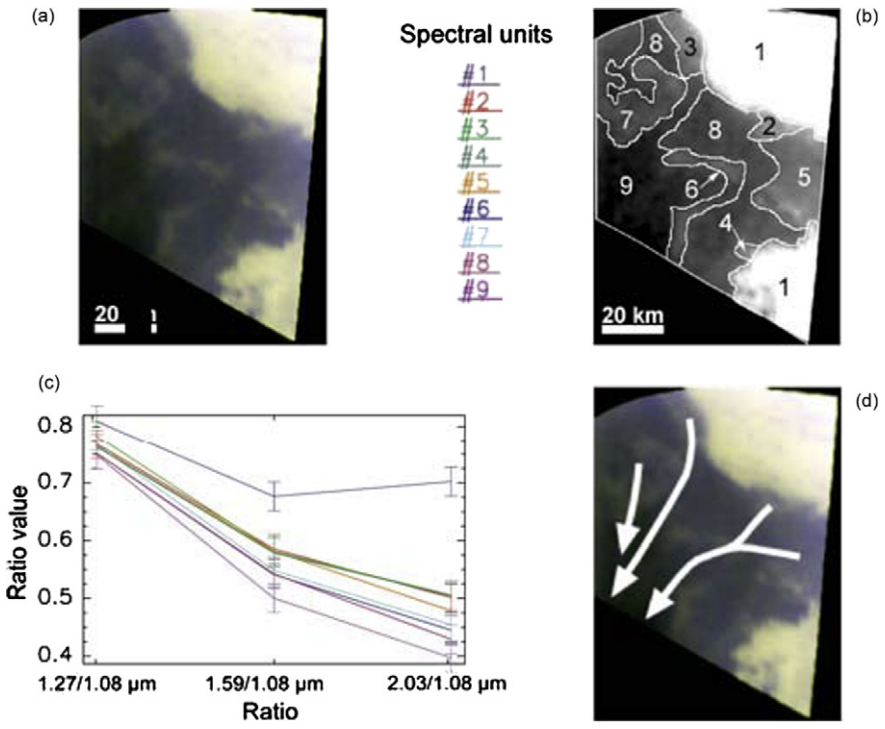

Fig. 7. Bright material is separated from dark material through a distinct boundary (a). Within the dark materials eight spectral units (b and c) are identified. The measurement accuracy of the spectral slopes (c) is 0.05, grouping the 9 units into 4 major classes. Absorptions and spectral slopes increase from the brightest to the darkest parts as shown by the northeast–southwest trending arrows in (d) indicating a change in composition, density and/or particle size.

scene. When applying PCT to the 256 VIMS infrared channels (0.88 to 5.10 µm), the very first PC bands appear to be dominated by surface signatures (Stephan et al., 2008), while the residual bands just contain noise. By using an inverse PC transformation applied to the first PC bands that show a coherent pattern, the inherent noise of the hyperspectral cube can be significantly reduced. The best VIMS images in terms of contrast are acquired in the wavelength ranges of Titan's atmospheric windows. Thus image quality can be significantly improved by co-adding several channels within these methane transmission windows. In order to improve image sharpness and to emphasize surface features, we obtained our best results by co-adding up to 12 spectral channels. Additionally, we oversampled the actual cube resolution by a factor of four and applied a bilinear interpolation to smooth pixels. We obtained the sharpest color images by using a false RGB color composite of band ratios using the VIMS channels at 1.29/1.08, 2.03/1.27 and 1.59/1.27 µm (Fig. 6). Consequently, spectral heterogeneities can be detected based on this rationing technique.

5. Spectral mapping of surface features

Based on these ratios three spectral units can be distinguished: Whitish material mainly distributed in the topographically high areas; bluish material adjacent to the bright-to-dark boundaries, and brownish material that correlates with the sand seas (Soderblom et al., 2007; Lorenz et al., 2006; Barnes et al., 2007a). Although the spectral units are distinct, their composition is not known at this time (McCord et al., 2006). Bright materials may consist of precipitated aerosol dust composed of methane-derived organics (Soderblom et al., 2007) superimposed on water-ice bedrock. The bluish component might contain some water ice as its defining feature (Soderblom et al., 2007). It is no simple matter, however, to distinguish between specific organics and ices because all these molecules have comparable absorptions, resulting in similar spectral slopes. In addition, different particle sizes will have an effect on the depth of absorption bands and corresponding spectral slopes. Nevertheless, the spectral signatures are real and indicate compositional differences and/or changes in particle sizes.

The most prominent bluish disintegration area between bright and dark materials on Titan is expressed as an indentation at about 30° W and 7° S trending northwards into bright material (Fig. 6), called Bohai Sinus, with a length of about 100 km and a width of 90 km. At the eastern end of the sinus, a bright spot of about 60 by 40 km occurs clearly isolated from the main bright area by a dark strait 2 to 8 km wide. At the northern end of that island, "Pacman Bay," a 25 km wide protrusion separates the island from the northern bright terrain. The indentation appears bluish in the ratioed image (Fig. 6), which is characteristic for the southern boundary of the bright area, but transforms to the brownish coded dune material further south outside of the bay area. At the northern edge of the bright area, brownish coded dune-like materials directly contact the bright border and thus clearly distinguish from its bluish southern counterpart. The bluish signature of Pacman Bay is spectrally identical with the surroundings of the Sinlap crater further northeast (Fig. 6) that is almost dune free and is supposed to consist of a higher water ice content due to ejected subsurface ice (Le Mouélic et al., 2008; Soderblom et al., 2007). The spectrally bluish units mark a transition zone between the bright material and the equatorial dune materials and might be composed of accumulations of materials that are correlated to the bright area.

In order to map the 'Pacman Bay' area, we ratioed three VIMS band at 1.29, 1.59, and 2.03 µm with respect to the band at 1.08 µm amplifying the spectral differences (Fig. 7). Based on these ratios we are able to map distinct units. Bright unit #1 has a spectral slope significantly different from that in the darker areas indicating major differences in composition and/or particle-size distribution. Within the bluish area we can distinguish 8 spectral units that differ in the depth of the three absorptions and related spectral slopes (Fig. 7c). The brighter spots within the dark area do not share the spectral characteristic of clouds, observed at comparable lighting conditions that appear bright at 2.8 µm compared

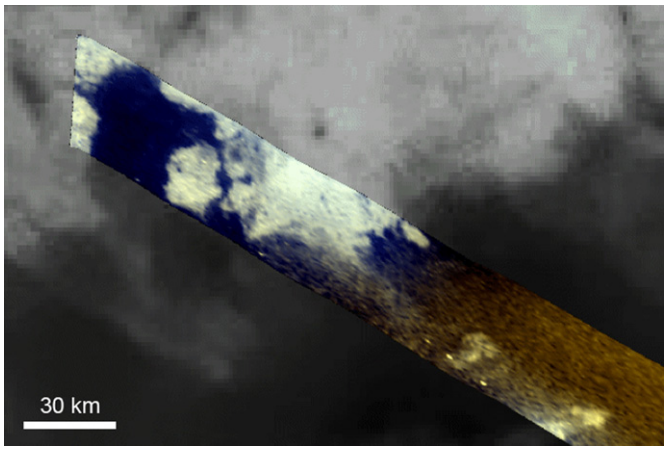

Fig. 8. Context view of the bluish transition area. Brownish dune material lies clearly outside the bluish zone (VIMS observation over ISS data (orbit T20)). VIMS wavelength ratios at 1.29/1.08, 2.03/1.27 and 1.59/1.27 μm have been composed to form blue, green and red color images in order to enhance the overall spectral contrast and distinguish between bright high-standing material, bluish areas and brownish dune material.

to 2.7 μm and are also bright at 5 μm, making surface features a reasonable interpretation for this observation. Units #2, #3 and #4 are very similar in their spectral characteristics and directly contact the bright material diffusing the sharp bright to blue boundary. Unit #5 is similar to these features, but it has a steeper 1.59 to 2.03 μm slope and a larger extent. Units #6, #7 and #8 are spectrally similar, with a slope comparable with that of units #2–#4, but are overall darker. Concerning their extent they are comparable with unit #5. In addition, unit #6 has a v-shaped structure also observable at the Huygens landing site (Tomasko et al., 2005). Unit #9 is darkest and has the steepest spectral slopes. Unit #9 is farthest from the bright material of unit #1 and merge into the brownish, dune-like material at the end of the sinus region (Fig. 6). Taking into account the error (Fig. 7c), the units group into four major classes: the bright materials of unit #1, lighter bluish material adjacent to the bright material as defined by units #2, #3, #4, and unit #5, the lighter bluish materials inside the bay reflected by units #6, #7, and #8, and finally the dark bluish material of unit #9. At the edge of the dark bluish zones (Fig. 8), brownish, sand-sized particles are piled into dunes by equatorial winds. The spectral characteristics change systematically from units #1 to #9 following the direction from northeast to southwest by a decrease in albedo and spectral slope (see arrows in Fig. 7d). This might be due to a selective separation of materials, either caused by density differences [e.g. the densities of liquid methane (National Institute of Standards and Technology, 2005), water-ice (National Institute of Standards and Technology, 2005; Burr et al., 2006) and organics (Hanley et al., 1977; Khare et al., 1994)] at 95 K and 1.6 bar are 450, 992 and 1500 kg/m^3, respectively, and/or different particle sizes, as it can be observed at the Huygens landing site. Thus the bluish zone resembles an area where material is spectrally arranged in a systematic way, clearly separated form the bright high-standing units and the dune covered areas.

6. Discussion

However, before we will understand these spectral correlations, we have to compare it with processes that can displace icy bedrock materials and rearrange them in a systematic manner. The major processes for dislocating surface material are aeolian, glacial and fluvial erosion and transport.

The dune-free characteristics (Fig. 8) and the systematic albedo and spectral slope pattern of Pacman Bay (Figs. 6 and 7), which contradict a usually random distribution of windblown deposits, do not support an aeolian origin of these materials. In particular, the clear spectral distinction between the bluish and the brownish materials in the color ratios (Figs. 6 and 8) suggests that these are two separate surface units caused by different forming processes. Soderblom et al. (2007) demonstrated, based on RADAR and VIMS data, that bluish areas are completely uncovered by dune material that abruptly terminates at this specific spectral boundary.

A glacial deposit might be consistent with the albedo features seen in Pacman Bay. Units #2 to #5 might be interpreted as ice avalanches and the v-shape of units #6 and #7 might resemble moraine-like deposits as formed by propagation and retreat of glaciers. However, similar features at the Huygens landing site do not show a correlation with glacial processes (Tomasko et al., 2005) and are not interpreted to be glacial in origin. In addition, the usually poorly sorted characteristic of glacial deposits contradicts the systematic spectral slope pattern. Glacial features are also not reported from RADAR or other VIMS observations so far, nor are they thermodynamically expected in the present climate (Lorenz and Lunine, 1996) and the surrounding of Pacman Bay do not show any evidence for glacial movement.

On the other hand, we have evidence of fluvial processes at the Huygens landing site and places elsewhere on Titan (Porco et al., 2005; Tomasko et al., 2005; Stofan et al., 2006; Perron et al., 2006; Barnes et al., 2007a, 2007b; Lorenz et al., 2008a).

The systematic spectral pattern and albedo variations of the units at Pacman Bay, which seems to be due to systematic changes of composition and/or particle size, as well as their position between the high-standing lands in the north and the dunes in the south (Fig. 6) suggest a deposition of materials that have accumulated during the low-velocity phase at end-of-flooding events. Thus, units #2, #3 #4 and #5 might be the accumulations of large-sized sediments directly at the contact to the bright materials presumably in regions where sediment loaded liquids enter the bay area, comparable to the proximal zone of an outwash plain (Benn and Evans, 1998). Units #6, #7 and #8 are similar to areas identified at the Huygens landing site (Tomasko et al., 2005) and particularly the v-shaped structure of unit #6 may indicate some flow-velocity-dependent accumulation of materials.

Units #9 is farthest from the bright material of unit #1 and merge into the brownish area at the end of the sinus (Figs. 6 and 8), where sand-sized particles are piled into dunes by equatorial winds. In terms of outwash plains this is consistent with a distal zone that mostly contains fine materials (Benn and Evans, 1998). Thus, the systematic change of the spectral characteristics of Pacman Bay is most likely consistent with a fluvial origin of the sediment, where material settles systematically dependent on the physical properties of the transported load. The total area of the bluish accumulation zone tending south from Pacman Bay to the brownish dune covered area (Figs. 6 and 8) extends over 20,000 km^2 indicating an extended sediment accumulation zone.

The material covering the bluish plains apparently originates from the bright Quivira Region (Fig. 6) surrounding Pacman Bay. However, due to the limited image resolution (500 m/pixel) of the VIMS data, deducing the processes responsible for sediment-loaded liquid release to Pacman Bay is not simple. Fluvial erosion can be triggered either by precipitation or cryovolcanic liquid release or can be connected to glacial processes.

As there is no evidence for glacial processes, subglacial liquid release is unlikely as well as liquid release caused by seasonal thawing because these processes are not reported from the Huygens landing site and so far are not observed elsewhere on Titan.

Cryovolcanic induced melting (Sotin et al., 2005) can produce a sudden release of large amounts of liquids that form in combination with unconfined material lahar-like mud flows (Fortes and Grindrod, 2006). Within such flows material settles out while flow

velocity decreases providing systematic sediment characteristics as observed in the bluish plains. Nevertheless, the major argument against the cryovolcanic–tectonic explanation is the lack of large volcanic constructs in the regions adjacent to Pacman Bay.

To account for the widespread plain deposits of fine-grained material release of large fluid volumes are required. High-energy flow will cause mechanical weathering and large accumulations of fine material in alluvial fans that can contribute to build dunes at least in the transition zone between the bluish plains and vast dune fields. Violent equatorial storms with heavy rainfall of methane explain this erosional process.

The most evident process for such erosional dislocation of material might be surface flow induced by precipitation, as indicated by the valley systems at the Huygens landing site and elsewhere on Titan (see discussion above). However, the details of the sediment formation process are presently less clear—although Collins (2005) has noted that the ice at these temperatures has rather similar mechanical properties to soft rocks on Earth.

The bright areas surrounding Pacman Bay are not homogeneous in contrast but show dark, bluish dissections and branching features. These darker elongated features within bright areas can be found elsewhere in ISS and VIMS observations from Titan's equatorial region and have been identified in a comparison with RADAR data as incised sinuous "valleys" that seem to result from surface runoff (Porco et al., 2005; Stofan et al., 2006; Barnes et al., 2007a, 2007b). The similarity between dark branching depressions from different locations within Titan's bright regions make it reasonable to assume that these features have a common origin and, by analogy to the Huygens landing site, the dominant baseline-forming process for all of these dark elongated sinuous depressions within bright terrain might be fluvial erosion. The dark sinuous features in bright regions might be comparable to high-order valleys of run-off systems. Can the faint bluish features, dissecting the bright materials adjacent to Pacman Bay, also be valleys? Unfortunately, the resolution of the VIMS observations of Pacman Bay is at the lower limit for identifying channels. In order to search for dark sinuous valley-like features in the bright surroundings of Pacman Bay, we improved the VIMS data by applying co-adding of band passes, rationing and spatial filtering, particularly of the bright areas. Thus, small differences in brightness and contrast can be identified and traced by plotting sets of parallel cross sections. Individual minima of the cross sections can be correlated as adjacent data points that follow an elongated sinuous pattern of dark depressions (Fig. 9). In comparison with dark sinuous channels identified elsewhere in VIMS and RADAR observations (Barnes et al., 2007a, 2007b) and with dark channels at the Huygens landing site, the dark features at Pacman Bay might be interpreted as segments of channels dissecting bright areas. In Fig. 9 we tried to map the widest segments marked with letters *a* to *h*. However, the segments do not convincingly resemble branching systems and we have to conclude, that, if there are valleys networks in this region, their width amounts to less than a VIMS pixels (<500 m) because a few kilometer wide valleys should occur in the VIMS data. Based on this assumption we can constrain a discharge-model for these 'hypothetical' valley systems with active channel width of <200 m. According to the discussions above, discharges of channels of such a valley system range from 100 m^3/s for short recurrence intervals to 1500 m^3/s (10 yr), 3000 m^3/s (100 yr) and 5100 m^3/s (1000 yr), respectively. The estimation of a drainage area is even more difficult and can only be constrained by general considerations. Within the equatorial plains, brightness is indicative for the topographic position. In first order, a decrease of brightness might roughly reflect the general slope. An ISS image mosaic (N1492350285, N1492350406, N1492350527) provides a resolution of 3 km/pixel for the northeastern context, indicating that the brightest region in the VIMS high resolution image (Fig. 10) is the southwestern part of a northeast tending bright ridge (dotted line in Fig. 10), which is probably the highest feature in the northern surroundings of Pacman Bay. The area with decreasing brightness towards the bay is indicated in Fig. 10 by dashed lines and can roughly be constrained to about 320 km^2. Thus, a 'hypothetical' valley system north of 'Pacman Bay,' would produce surface run-off rates of about 3 cm/day (1.2 mm/h) for short recurrence intervals and 40 cm/day (17 mm/h) to 140 cm/day (60 mm/h) for longer recurrence intervals. Even the run-off rates of short recurrence intervals would be sufficient to move particles up to the size of a centimeter (Perron et al., 2006). According to a precipitation triggered run-off model for Pacman Bay as described above, the erosional parameters are compatible with discharges and run-off rates needed to move sediment (Burr et al., 2006; Perron et al., 2006) as well as the expected precipitation rates (Hueso and Sanchez-Lavega, 2006).

Although, we cannot undoubtedly identify the erosional process that is responsible for the formation of the accumulation plains in 'Pacman Bay,' fluvial surface run-off of sediment-loaded liquid is compatible with the spectral observations and liquid release by precipitation and surface run-off seems feasible to explain these observation.

7. Conclusions

Titan exhibits valley networks indicating erosion by surface run-off as well as accumulation zones with a systematic separation of materials. Both observations support high erosion efficiency on Titan, causing intense mechanical degradation and production of fine-clastic debris that is transported along the local slopes. Discharges and runoff production rates are sufficient to move particles of up to a few tens of centimeters as observed at the Huygens landing site by assuming shallow flow depth and frictional shear velocities of <10 cm/s (Perron et al., 2006; Burr et al., 2006). The estimated runoff production rates range between 0.1–20 mm/h for extended systems and peak rates between 60–400 mm/h for the small steep sloped systems at the Huygens landing site (Table 2) with the higher values are related to longer recurrence intervals (>100 years). This is consistent with the rates (0.5–15 mm/h) needed to move sediment of the size of 1–15 mm (Perron et al., 2006). Modeled methane convective storms on Titan, having rainfall of 110 kg/m^2 within 5–8 h (20–50 mm/h) (Hueso and Sanchez-Lavega, 2006), are sufficient to trigger such flash floods. Even moderate storms with rainfall of 30 kg/m^2 within 5–10 h (6–12 mm/h) will explain the observed run-off rates. On the other hand, precipitation rates as estimated from the current atmospheric conditions might not exceed 1 cm/yr (Lorenz, 2000; Rannou et al., 2006; Tokano et al., 2006), comparable to terrestrial deserts. To satisfy the overall energy balance of the hydrological cycle, the heavy rainstorms indicated above must be infrequent—perhaps centuries apart, which is consistence with the estimated run-off production rates. Even if we assume low drizzling rates (Tokano et al., 2006), long-term accumulation of liquid in the subsurface might be subject to the formation of large reservoirs in the underground and possible volcanic or tectonic triggered sudden jökuhllhaup-like (Benn and Evans, 1998) release of large amount of liquids. Low precipitation rates might also be restricted to the current dry season that actually switches from summer to winter. However, we cannot exclude cryovolcanic and tectonically induced melting (Sotin et al., 2005) to be responsible for sudden release of large amounts of liquids that form in combination with unconfined material, lahar-like mud flows (Fortes and Grindrod, 2006) or hyper-concentrated flows that can also cause the observed sedimentation in Pacman Bay. Nevertheless, the major argument

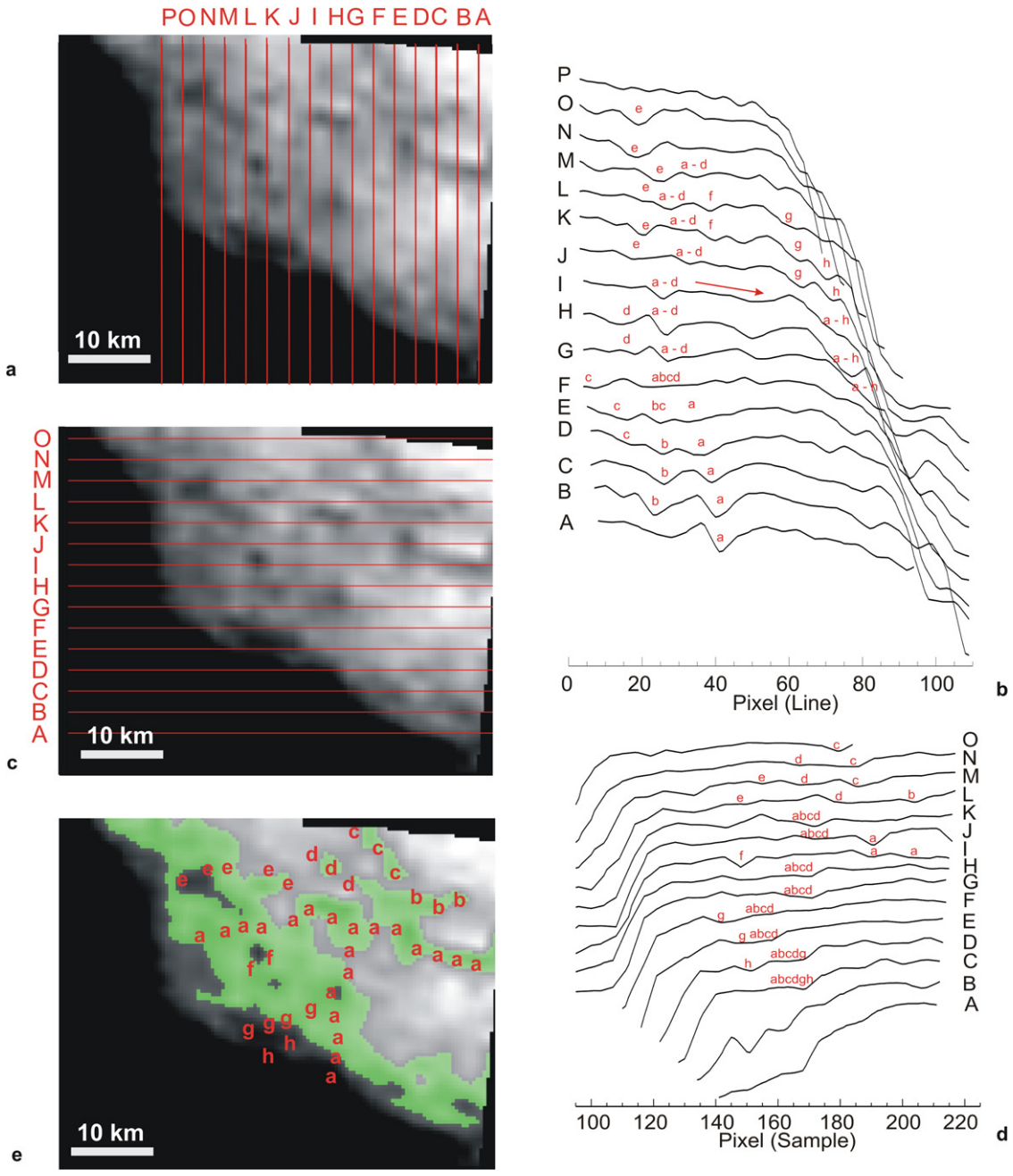

Fig. 9. The bright area bordering the northern part of Pacman Bay exhibits elongated sinuous dark albedo marks that dissect the surface and can be identified in the N–S (a) and E–W (c) brightness cross sections (b, d). The v-shaped low-albedo features in the cross-sections of (b) and (d), are mapped in (e). Although the low albedo features correlated to some extent a branching system cannot be identified at this scale. Thus 'hypothetic' valley networks must be smaller than the VIMS resolution.

against the cryovolcanic–tectonic explanation is the lack of large volcanic constructs in this area. In order to produce the sediment covering, the bluish accumulation zone (Figs. 6 and 8) requires frequent eruptions that should build observable volcanic constructs.

On the other hand, weather conditions can easily change within a short timescale. The existing database suggests that frequent and heavy precipitation is the most feasible process to explain runoff and erosion. Convection-driven rainstorms and precipitation-induced flooding are also consistent with the recently discovered northern-hemispherical lakes (Stofan et al., 2007). However, because erosional and depositional processes are found in the equatorial regions whereas lakes are in the polar regions and since recent large-scale storm activity was concentrated near the South Pole we cannot decide at this stage whether the observed erosion was mainly driven by plaeoclimatic processes or is a seasonal effect or is due to volcanic outgassing and to what extend these processes cause the surface erosion to cease. More global and timely repeated observations of erosional features are needed to further constrain the global circulation and the related methane cycle with time.

Acknowledgments

We gratefully acknowledge the long years of work by the entire Cassini team that allowed these data of Titan to be obtained. We also acknowledge NASA, ESA, DLR, ASI, CNES, JPL, and the University of Arizona that provide support for the international VIMS team. We thank K.D. Matz for data processing support and also K.P. Harrison and an anonymous reviewer for their discussions.

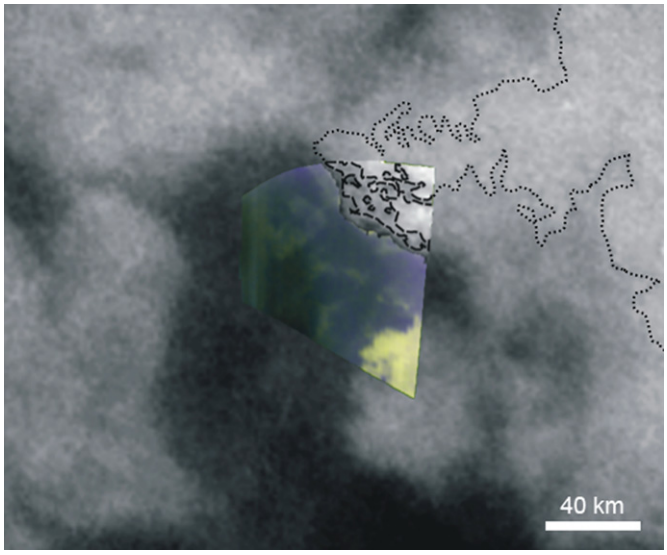

Fig. 10. The drainage area bordering Pacman Bay to the north can be defined based the VIMS image from orbit T20 (resolution 500 m/pixel). The dashed line encloses the area where channels are found. In order to provide a broader context the high resolution VIMS image is overlaid on an ISS near infrared (0.938 μm) image mosaic (N1492350285, N1492350406, N1492350527; orbit 006TI) with a resolution of about 3 km/pixel. According to the brightness distribution in the lower resolved ISS images, the highest (brightest) peak of the drainage area is located just in the northeast of the VIMS high-resolution image (dotted line). The distance from the southeastern edge of this ridge to Pacman Bay is about 30 km and the drainage area (dashed line) covers about 320 km^2.

References

Barnes, J.W., Brown, R.H., Soderblom, L., Buratti, B.J., Sotin, C., Rodriguez, S., Le Mouèlic, S., Baines, K.H., Clark, R., Nicholson, P., 2007a. Global-scale surface spectral variations on Titan seen from Cassini/VIMS. Icarus 186, 242–258.

Barnes, J.W., Radebaugh, J., Brown, R.H., Wall, S., Soderblom, L., Lunine, J., Burr, D., Sotin, C., Le Mouèlic, S., Rodriguez, S., Buratti, B.J., Clark, R., Baines, K.H., Jaumann, R., Nicholson, P.D., Kirk, R.L., Lopes, R., Lorenz, R.D., Mitchell, K., Wood, C.A., the Cassini RADAR team, 2007b. Near-infrared spectral mapping of Titan's mountains and channels. J. Geophys. Res. 1112, doi:10.1029/2007JE002932. E11006.

Benn, D.I., Evans, D.J.A., 1998. Glaciers and Glaciation. Arnold, London. 734 pp.

Brown, R.H., Baines, K.H., Bellucci, G., Bibring, J.-P., Buratti, B.J., Bussoletti, E., Capaccioni, F., Cerroni, P., Clark, R.N., Coradini, A., Cruikshank, D.P., Drossart, P., Formisano, V., Jaumann, R., Langevin, Y., Matson, D.L., McCord, T.B., Miller, E., Nelson, R.M., Nicholson, P.D., Sicardy, B., Sotin, C., 2004. The Cassini visual and infrared mapping spectrometer investigation. Space Sci. Rev. 115, 111–168.

Burr, D.M., 2007. Fluvial flow on Titan: Context for geomorphic interpretation. In: Workshop on: Ices, Oceans, and Fire: Satellites of the outer Solar System. LPI Contribution No. 1357.

Burr, D.M., Emery, J.P., Lorenz, R.D., Collins, G.C., Carling, P.A., 2006. Sediment transport by liquid surficial flow: Application to Titan. Icarus 181, 235–242.

Collins, G.C., 2005. Relative rates of fluvial incision on Titan and Earth. Geophys. Res. Lett. 32, doi:10.1029/2005GL024551.

Elachi, C., Wall, S., Allison, M., Anderson, Y., Boehmer, R., Callahan, P., Encrenaz, P., Flamini, E., Francescetti, G., Gim, Y., Hamilton, G., Hensley, S., Janssen, M., Johnson, W., Kelleher, K., Kirk, R., Lopes, R., Lorenz, R., Lunine, J., Muhleman, D., Ostro, S., Paganelli, F., Picardi, G., Posa, F., Roth, L., Seu, R., Shaffer, S., Soderblom, L., Stiles, B., Stofan, E., Vetrella, S., West, R., Wood, C., Wye, L., Zebker, H., 2005. Cassini radar views the surface of Titan. Science 308, 970–974.

Elachi, C., Wall, S., Janssen, M., Stofan, E., Lopez, R., Kirk, R., Lunine, J., Paganelli, F., Soderblom, L., Wood, C., Wye, L., Zebker, H., Anderson, Y., Ostro, S., Allison, M., Callahan, P., Encrenaz, P., Flamini, E., Francescetti, G., Gim, Y., Hamilton, G., Hensley, S., Johnson, W., Kelleher, K., Muhleman, D., Picardi, G., Posa, F., Roth, L., Seu, R., Shaffer, S., Stiles, B., Vetrella, S., West, E., 2006. Titan radar mapper observations from Cassini's T3 fly-by. Nature 441, 709–713.

Fortes, A.D., Grindrod, P.M., 2006. Modeling of possible mud volcanism on Titan. Icarus 182, 550–558.

Hanley, H.J.M., Haynes, W.M., McCarty, R.D., 1977. The viscosity and thermal conductivity coefficient for dense gaseous and liquid methane. J. Phys. Chem. Ref. Data 6, 597–601.

Hueso, R., Sanchez-Lavega, A., 2006. Methane storms on Saturn's moon Titan. Nature 442, 428–431.

Irwin, R.P.R., Craddock, A., Howard, H.D., 2005. Interior channels in martian valley networks: Discharge and runoff production. Geology 33, 489–492.

Jaumann, R., Stephan, K., Brown, R.H., Buratti, B.J., Clark, R.N., McCord, T.B., Coradini, A., Capaccioni, P., Filacchione, G., Cerroni, P., Baines, K.H., Bellucci, G., Bibring, J.P., Combes, M., Cruikshank, D.P., Drossart, P., Formisano, V., Langevin, Y., Matson, D.L., Nelson, R.M., Nicholson, P.D., Sicardy, B., Sotin, C., Soderblom, L.A., Griffith, C., Matz, K.D., Roatsch, T., Scholten, F., Porco, C.C., 2006. High-resolution Cassini-VIMS mosaics of Titan and the icy saturnian satellites. Planet. Space Sci. 54, 1146–1155.

Khare, B.N., Sagan, C., Thompson, W.R., Arakawa, E.T., Meisse, C., Tuminello, P.S., 1994. Optical properties of poly-HCN and their astronomical applications. Can. J. Chem. 72, 678–694.

Kleinhans, M.G., 2005. Flow discharge and sediment transport models for estimating a minimum timescale of hydrological activity and channel and delta formation on Mars. J. Geophys. Res. 110, doi:10.1029/2005JE002521. E12003.

Komar, P., 1980. Modes of sediment transport in channelized water flows with ramifications to the erosion of martian outflow channels. Icarus 42, 317–329.

Le Mouélic, S., Paillou, P., Janssen, M.A., Barnes, J.W., Rodriguez, S., Sotin, C., Brown, R.H., Baines, K., Buratti, B.J., Clark, R.N., Crapeau, M., Encrenaz, P.J., Jaumann, R., Geudtner, D., Paganelli, F., Soderblom, L., Tobie, G., Wall, S., 2008. Mapping and interpretation of Sinlap crater on Titan using Cassini VIMS and Radar data. J. Geophys. Res., in press.

Leopold, L.B., Wolman, M.G., Miller, J.P., 1964. Fluvial Processes in Geomorphology. W.H. Freeman and Company, San Francisco.

Lopes, R., Mitchell, K.L., Stofan, E.R., Lunine, J.I., Lorenz, R., Paganelli, F., Kirk, R.L., Wood, C.A., Wall, S.D., Robshaw, L.E., Fortes, A.D., Neish, C.D., Radebaugh, J., Reffet, E., Ostro, S.J., Elachi, C., Allison, M.D., Anderson, Y., Boehmer, R., Boubin, G., Callahan, P., Encrenaz, P., Flamini, E., Francescetti, G., Gim, Y., Hamilton, G., Hensley, S., Janssen, M.A., Johnson, W.T., Kelleher, K., Muhleman, D.O., Ori, G., Orosei, R., Picardi, G., Posa, F., Roth, L.E., Seu, R., Shaffer, S., Soderblom, L.A., Stiles, B., Vetrella, S., West, R.D., Wye, L., Zebker, H.A., 2007. Cryovolcanic features on Titan's surface as revealed by the Cassini Titan Radar Mapper. Icarus 186, 395–412.

Lorenz, R.D., 2000. The weather on Titan. Science 290, 467–468.

Lorenz, R.D., Lunine, J.I., 1996. Erosion on Titan: Past and present. Icarus 122, 79–91.

Lorenz, R.D., Wall, S., Radebaugh, J., Boubin, G., Reffet, E., Janssen, M., Stofan, E., Lopez, R., Kirk, R., Elachi, C., Lunine, J., Mitchell, K., Paganelli, F., Soderblom, L., Wood, C., Wye, L., Zebker, H., Anderson, Y., Ostro, S., Allison, M., Boehmer, R., Callahan, P., Encrenaz, P., Ori, G.G., Francescetti, G., Gim, Y., Hamilton, G., Hensley, S., Johnson, W., Kelleher, K., Muhleman, D., Picardi, G., Posa, F., Roth, L., Seu, R., Shaffer, S., Stiles, B., Vetrella, S., Flamini, E., West, R., 2006. The sand seas of Titan: Cassini RADAR observations of longitudinal dunes. Science 312, 724–727.

Lorenz, R.D., Lopes, R.M., Paganelli, F., Lunine, J.I., Kirk, R.L., Mitchell, K.L., Soderblom, L.A., Stofan, E.R., Ori, G., Myers, M., Miyamoto, H., Radebaugh, J., Stiles, B., Wall, S.D., Wood, C.A., the Cassini RADAR team, 2008a. Fluvial channels on Titan: Initial Cassini RADAR observations. Planet. Space Sci. 56, 1132–1144.

Lorenz, R.D., Mitchell, K.L., Kirk, R.L., Hayes, A.G., Zebker, H.A., Paillou, P., Radebaugh, J., Lunine, J.I., Janssen, M.A., Wall, S.D., Lopes, R.M., Stiles, B., Ostro, S., Mitri, G., Stofan, E.R., the Cassini RADAR team, 2008b. Titan's inventory of organic surface materials. Geophys. Res. Lett. 35, doi:10.1029/2007GL032118. L02206.

Lunine, J.I., 1993. Does Titan have an ocean? Review of current understanding of Titan's surface. Rev. Geophys. 31, 133–149.

McCauley, J.F., Carr, M.H., Cutts, J.A., Hartmann, W.K., Masursky, H., Milton, D.J., Sharp, R.P., Wilhelms, D.E., 1972. Preliminary Mariner 9 Report on the geology of Mars. Icarus 17, 289–327.

McCord, T.B., Hansen, G.B., Buratti, B.J., Clark, R.N., Cruikshank, D.P., D'Aversa, E., Griffith, C.A., 2006. Composition of Titan's surface from Cassini VIMS. Planet. Space Sci. 54, 1524–1539.

Moore, J.M., Howard, A.D., Dietrich, W.E., Schenk, P.M., 2003. Martian layered fluvial deposits: Implications for Noachien climate scenarios. Geophys. Res. Lett. 30 (24), doi:10.1029/2003GL019002. 2292.

National Institute of Standards and Technology (NIST), 2005. Chemistry Web Book, Standard Reference Data Base, no. 69, June 2005. http://webbook.nist.gov/chemistry.

Osterkamp, W.R., Hedman, E.R., 1982. Perenial-streamflow characteristics related channel geometry and sediment in Missouri River Basin. US Geol. Surv. Prof. Paper 1242.

Perron, J.T., Lamb, M.P., Koven, C.D., Fung, I.Y., Yager, E., Ádámkovics, M., 2006. Valley formation and methane precipitation rates on Titan. J. Geophys. Res. 111, doi:10.1029/2005JE002602. E11001.

Porco, C.C., Baker, E., Barbara, J., Beurle, K., Brahic, A., Burns, J.A., Charnoz, S., Cooper, N., Dawson, D.D., Del Genio, A.D., Denk, T., Dones, L., Dyudina, U., Evans, M.W., Fussner, S., Giese, B., Grazier, K., Helfenstein, P., Ingersol, A.P., Jacobson, R.A., Johnson, T.V., McEwen, A., Murray, C.D., Neukum, G., Owen, W.M., Perry, J., Roatsch, T., Spitale, J., Squyres, S., Thomas, P., Tiscareno, L., Turtle, E.P., Vasavada, A.R., Veverka, J., Wagner, R., West, R., 2005. Imaging of Titan from the Cassini spacecraft. Nature 434, 159–168.

Radebaugh, J., Lorenz, R.D., Kirk, R.L., Lunine, J.I., Stofan, E.R., Lopez, R.M.C., Wall, S.D., the Cassini RADAR team, 2007. Mountains on Titan observed by Cassini radar. Icarus 192, 77–91.

Rannou, P., Montmessin, F., Hourdin, F., Lebonnois, S., 2006. The latitudinal distribution of clouds on Titan. Science 311, 201–205.

Richards, J.A., 1994. Remote Sensing Digital Image Analysis: An Introduction. Springer-Verlag, Berlin, Germany. 340 pp.

Rothery, D.A., Hunt, G.A., 1990. A simple way to perform decorrelation stretching and related techniques on menu-driven image processing systems. Int. J. Remote Sens. 11, 133–137.

Silberman, E., Carter, R., Einstein, H., Hinds, J., Powell, R., ASCE, 1963. Task force on friction factors in open channels. J. Hydraul. Eng. 89 (HY2), 97–143.

Soderblom, L., Anderson, J., Baines, K., Barnes, J., Barrett, J., Brown, R.H., Buratti, B., Clark, R., Cruikshank, D., Elachi, C., Janssen, M., Jaumann, R., Kirk, R., Karkoschka, E., Lemouelic, S., Lopes, R., Lorenz, R., Lunine, J., McCord, T., Nicholson, P., Radebaugh, J., Rizk, B., Sotin, C., Stofan, E., Sucharski, E.T., Tomasko, M., Wall, S., 2007. Correlations between Cassini VIMS spectra and RADAR SAR images: Implications for Titan's surface composition and the character of the Huygens Probe landing site. Planet. Space Sci. 55, 2025–2036.

Sotin, C., Jaumann, R., Buratti, B.J., Brown, R.B., Clark, R.N., Soderblom, L.A., Baines, K.H., Bellucci, G., Bibring, J.-P., Capaccioni, F., Cerroni, P., Coradini, A., Cruikshank, D.P., Drossart, P., Formisano, V., Langevin, Y., Matson, D.L., McCord, T.B., Nelson, R.M., Nicholson, P.D., Sicardy, B., LeMouelic, L., Rodriguez, S., Stephan, K., Scholz, C.K., 2005. Release of volatiles from a possible cryovolcano from near-infrared imaging of Titan. Nature 435, 786–789.

Stephan, K., Hibbitts, C.A., Hoffmann, H., Jaumann, R., 2008. Reduction of instrument dependent noise in hyperspectral image data using the principal component analysis—Application to Galileo NIMS data. Planet. Space Sci. 56, 406–419.

Stofan, E.R., Lunine, J.I., Lopes, R., Paganelli, F., Lorenz, R.D., Wood, C.A., Kirk, R., Wall, S., Elachi, C., Soderblom, L.A., Ostro, S., Janssen, M., Radebaugh, J., Wye, L., Zebker, H., Anderson, Y., Allison, M., Boehmer, R., Callahan, P., Encrenaz, P., Flamini, E., Francescetti, G., Gim, Y., Hamilton, G., Hensley, S., Johnson, W.T.K., Kelleher, K., Muhleman, D., Picardi, G., Posa, F., Roth, L., Seu, R., Shaffer, S., Stiles, B., Vetrella, S., West, R., 2006. Mapping of Titan: Results from the first Titan radar passes. Icarus 185, 443–456.

Stofan, E.R., Elachi, C., Lunine, J.I., Lorenz, R.D., Stiles, B., Mitchell, K.L., Ostro, S., Soderblom, L., Wood, C., Zebker, H., Wall, S., Janssen, M., Kirk, R., Lopes, R., Paganelli, S., Radebaugh, J., Wye, L., Anderson, Y., Allison, M., Boehmer, R., Callahan, P., Encrenaz, P., Flamini, E., Francescetti, G., Gim, Y., Hamilton, G., Hensley, S., Johnson, W.T.K., Kelleher, E., Muhleman, D., Paillou, P., Picardi, G., Posa, F., Roth, L., Seu, R., Shaffer, S., Vetrella, S., West, R., 2007. The lakes of Titan. Nature 445, 61–64.

Thekekara, M.P., 1973. Solar energy outside the Earth's atmosphere. Sol. Energy 14, 109–127.

Tokano, T., 2001. Modeling of thunderclouds and lightning generation on Titan. Planet. Space Sci. 49, 539–560.

Tokano, T., McKay, C.P., Neubauer, F.M., Atreya, S.K., Ferri, F., Fulchignoni, M., Niemann, H.B., 2006. Methane drizzle on Titan. Nature 442, 432–435.

Tomasko, M.G., Archinal, B., Becker, T., Bézard, B., Bushroe, M., Combes, M., Cook, D., Coustenis, A., de Bergh, C., Dafoe, L.E., Doose, L., Douté, S., Eibl, A., Engel, S., Gliem, F., Grieger, B., Holso, K., Howington-Kraus, E., Karboschka, E., Keller, H.U., Kirk, R., Kramm, R., Küppers, M., Lanagan, P., Lellouche, E., Lemmon, M., Lunine, J., McFarlane, E., Moores, J., Prout, G.M., Rizk, B., Rosiek, M., Rueffer, P., Schröder, S.M., Schmitt, B., See, C., Smith, P., Soderblom, L., Thomas, N., West, R., 2005. Rain, wind and haze during the Huygens probe's decent to Titan's surface. Nature 438, 765–778.

William, G.P., 1988. Paleofluvial estimates from dimensions of former channels and meanders. In: Baker, V.R., Kochel, R.C., Patton, P.C. (Eds.), Flood Geomorphology. Wiley, New York, pp. 321–334.

Wilson, L., Ghatan, G.J., Head III, J.W., Mitchell, K.L., 2004. Mars outflow channels: A reappraisal of the estimation of water flow velocities from water depth, regional slopes, and channel floor properties. J. Geophys. Res. 109, doi:10.1029/2004JE002281. E09003.

Zarnecki, J.C., Leese, R.M., Hathi, B., Ball, A.J., Hagermann, A., Towner, M.D., Lorenz, R.D., McDonnell, T., Green, S.F., Patel, M.R., Ringrose, T.J., Rosenberg, P.D., Atkinson, K.R., Paton, M., Banaskiewicz, M., Clark, B.C., Ferri, F., Fulchignoni, M., Ghafoor, N.A.L., Kargl, G., Svedhem, H., Delderfield, J., Grande, M., Parker, D.J., Challenor, P., 2005. A soft solid surface on Titan at the Huygens landing site as measured by the Surface Science Package (SSP). Nature 438, 792–795.